Dyes and Pigments 81 (2009) 1–9

Contents lists available at ScienceDirect

Dyes and Pigments

journal homepage: www.elsevier.com/locate/dyepig

Spectroscopic and molecular modeling of the binding of *meso*-tetrakis(4-hydroxyphenyl)porphyrin to human serum albumin

Wenting An [a], Yong Jiao [a], Chuan Dong [a], Cheng Yang [b], Yoshihisa Inoue [b], Shaomin Shuang [a,*]

[a] Research Center of Environmental Science and Engineering, Department of Chemistry, Shanxi University, Taiyuan 030006, PR China
[b] Department of Applied Chemistry, Osaka University, Suita 565-0871, Japan

ARTICLE INFO

Article history:
Received 2 June 2008
Received in revised form 12 August 2008
Accepted 13 August 2008
Available online 22 August 2008

Keywords:
meso-Tetrakis(4-hydroxyphenyl)porphyrin (THPP)
Human serum albumin (HSA)
Steady-state fluorescence
Fourier transform infrared (FT-IR) spectroscopy
Circular dichroism (CD) spectroscopy
Molecular modeling

ABSTRACT

The binding of *meso*-tetrakis(4-hydroxyphenyl)porphyrin to human serum albumin has been investigated by the combination of fluorescence, UV–vis absorption, Fourier transform infrared, circular dichroism spectroscopies and molecular modeling. Fluorescence and UV–vis data indicated that hydrophobic interaction is the main driving force for binding and that aggregation of the colorant plays a major role in the affinity of the dye for the serum. The dye–serum distance, *r*, was determined to be ~4 nm based on Förster non-radiative energy transfer theory. FT-IR and CD spectral examinations revealed that binding induces a conformational change in the serum which reduces the α-helix structure of the protein. Molecular modeling suggested that the colorant can partially insert into the site II of subdomain IIIA via hydrophobic and hydrogen bonding interactions.

1. Introduction

There has been a growing interest in the use of porphyrins and their related compounds as therapeutic drugs, especially as photosensitizers in the photodynamic therapy (PDT) of cancer [1,2], where the combination of light and photosensitizer generates active oxygen species near the tumor to damage the malfunctioned tissues. A variety of porphyrins (anionic porphyrin [3], hematoporphyrin (Hp) [4], and cationic porphyrin [5]) and phthalocyanines [6] have been successfully used in clinical trials for tumor treatment. Porphyrins have recently been used in several model systems that mimic the biological electron and oxygen transport [7–9], as versatile probes for detecting the nucleic acid structure [10], and also in the treatment of viral and bacterial infections, including the HIV [11]. As one of the second-generation photosensitizers, *meso*-tetrakis(4-hydroxyphenyl)porphyrin (THPP, Fig. 1) with high photosensitivity and organic selectivity may be used as a potential drug molecule in PDT for anticancer treatment, and indeed a recent report has shown that THPP can destroy intrahepatic tumors with better efficacies and fewer side effects [12].

Porphyrins taken into the blood circulation system as tumor localizing photosensitizers for PDT are transported to target tissues by human serum albumin (HSA) and other plasma proteins such as low- and high-density lipoproteins. HSA is the most abundant plasma protein, which plays key roles in transport, distribution and metabolism of many endogenous and exogenous ligands, such as fatty acids, metabolites, and drugs [13]. The binding to HSA often changes the photophysical and photochemical properties of porphyrins [14], as a consequence of the interaction with the specific amino acids near the binding site. It is accepted that there are two major specific drug binding sites, site I and site II, in HSA, which are located in subdomain IIA and IIIA [15], respectively. Therefore, the understanding of the interaction of porphyrins with HSA is of utmost importance in formulating safe drugs and effective dosages. A wide variety of techniques have been exploited to investigate the binding behavior of ligand to protein, including UV–vis [16–18], fluorescence [17–22], infrared (IR) [21,22], and circular dichroism (CD) spectroscopies [18,21,22], as well as capillary electrophoresis [23], ^{1}H NMR spectroscopy [24], and molecular modeling [21,22]. Of these methods, we employed a combination of spectroscopic methods in the present work for their high sensitivity and accessibility.

We have previously reported the spectroscopic studies to characterize the interactions of some drugs with serum albumin [25,26]. In this study to elucidate the binding behavior of THPP to HSA, we wish to determine the binding constant and characterize the nature of the binding site at different pHs by the combined use

* Corresponding author. Tel.: +86 351 7018842; fax: +86 351 7011322.
E-mail address: smshuang@sxu.edu.cn (S. Shuang).

0143-7208/$ – see front matter © 2008 Elsevier Ltd. All rights reserved.
doi:10.1016/j.dyepig.2008.08.004

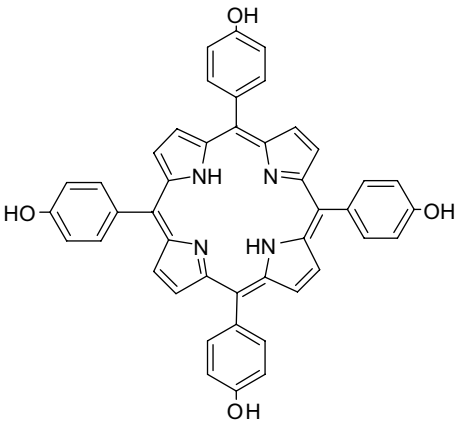

Fig. 1. The chemical structure of THPP.

of UV–vis, fluorescence, Fourier transform infrared (FT-IR), and circular dichroism (CD) spectroscopies, as well as molecular modeling examinations. The fluorescence and UV–vis spectral studies revealed that the binding process is highly dependent on the solution pH and the degree of THPP aggregation, while the FT-IR and CD spectral examinations showed that the binding of THPP to HSA induces a conformational change of HSA, probably loosening the α-helix structures of the protein. Molecular modeling was performed to explore the possible binding site and assess the microenvironment around the bound THPP. The binding properties of THPP to HSA elucidated in this study may provide some clues for future application of THPP as a photosensitizer in photodynamic therapy (PDT) for anticancer treatment.

2. Materials and methods

2.1. Materials

THPP was successfully synthesized by the literature procedure [27]. HSA was purchased from the Biological Identification Institute of Shanghai and L-tryptophan from the Institute of Microorganism of Chinese Academy of Science. HSA and THPP solutions were prepared by dissolving the solid samples in doubly distilled water and dimethylsulfoxide (DMSO), respectively. All other chemicals were of analytical grade and used without further purification. Doubly distilled water was used throughout the work and all stock solutions were stored at 0–4 °C.

2.2. Apparatus

UV–vis and fluorescence spectra were measured at 20 ± 1 °C in standard quartz cells of 1 cm path length on a Shimadzu UV-265 spectrophotometer and a Hitachi F-4500 spectrofluorimeter, respectively. Both of the excitation and emission bandwidths were set at 5 nm. FT-IR measurements were recorded at room temperature on a Nicolet Nexus 670 FT-IR spectrometer equipped with a germanium attenuated total reflection (ATR) accessory. Circular dichroism (CD) measurements were carried out on a JASCO 810 spectropolarimeter in a 1 cm quartz cell at room temperature. pH was measured by using a pH meter E-201-C made by the Factory of Magnetic Spectrograph, Shanghai.

2.3. Spectroscopic measurements

A 1 mL aliquot of the stock solution of THPP (5.0×10^{-5} mol L^{-1}) in DMSO was transferred to a 10 mL volumetric flask, to which was added an appropriate amount of 5.0×10^{-4} mol L^{-1} solution of HSA. The pH was controlled by adding 0.5 mL of a 0.5 mol L^{-1} phosphate buffer solution. The mixed solution was diluted to the final volume with double distilled water and the resulting solution was shaken thoroughly, and then the absorption or fluorescence spectra were measured after standing for 30 min.

FT-IR spectra were taken at 4 cm^{-1} resolution with 60 times repeated scans by using an attenuated total reflection (ATR) apparatus. The FT-IR spectrum of THPP-free HSA was acquired by subtracting the absorption of buffer solution from that of the protein solution, and the difference spectrum of THPP-bound HSA was obtained by subtracting the spectrum of THPP solution from that of THPP–HSA solution. The subtraction criterion was that the original spectrum of protein solution between 2200 and 1800 cm^{-1} was featureless [28]. Fourier self-deconvolution and secondary derivative methods were applied to the spectra in the range 1600–1700 cm^{-1} to estimate the number, position, and width of component bands. Based on these parameters a curve-fitting analysis was carried out by using the Galactic PeakSolve software (Nicolet) to get the best Gaussian-shaped curves that fit to the original protein spectrum. After identifying the individual bands, the representative structure of HSA was calculated using the area of their respective component bands.

CD spectra were obtained by subtracting the ellipticity of THPP from that of the THPP–HSA mixture at the same wavelength and the unit results are shown in millidegree. The α-helix content of HSA was analyzed by the secondary structure estimation module of the Spectra Manager software package (JASCO).

2.4. Molecular modeling

The potential of the 3D structure of HSA was assigned according to the CFF91 force field. The initial structure of THPP was generated by molecular modeling platform Insight II 2000 (Accelrys), and the geometries of the THPP were subsequently optimized by using the CFF91 force field. The docking method was used to calculate the binding modes of THPP with HSA. All calculations were performed on an SGI workstation.

3. Results and discussion

3.1. Complexation of the neutral form of THPP with HSA

Fig. 2 shows the absorption spectra of THPP in the presence of HSA of varying concentrations at pH 3.0. In acidic media, THPP exists in the acidic form, H_4THPP^{2+}, and its Soret band appears at 447 nm in the absence of HSA. Upon gradual addition of HSA, a new peak centered at 426 nm appeared at the expense of the original peak at 447 nm with accompanying isosbestic point at 433 nm, confirming the stoichiometric formation of the complex [29], as shown in Scheme 1. The Q band of the acidic form at 688 nm was decreased in intensity and split into four bands, indicating that THPP is bound to HSA not as a cation but as a neutral species. In view of the molecular structure and the nature of the THPP and HSA species existing in the acidic solution, it is unlikely that THPP is bound to HSA through a covalent bond. The binding of THPP to HSA is better explained by non-covalent interactions such as van der Waals, hydrogen bonding, and hydrophobic interactions [30]. Under the experimental condition (pH 3.0), some amino acid residues of HSA, such as lysine and arginine, are protonated due to the pH value being lower than the isoelectric point of HSA ($pI_{HSA} = 5.4$), meaning that the whole protein possesses net positive charges. At pH 3.0, THPP is also protonated and exists as a dication, and hence the approach of a positively charged THPP to a similarly charged HSA is electrostatically repulsive and the inclusion into HSA is not favored by the less hydrophobic nature of the charged THPP core. All of these factors drive the complexation of the neutral, rather

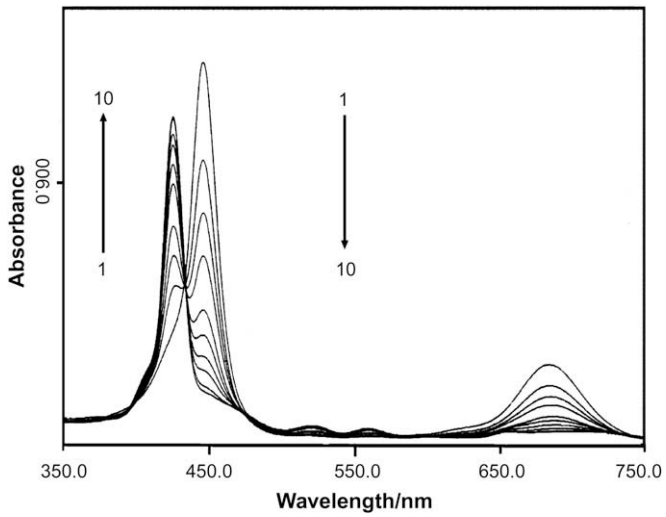

Fig. 2. UV–vis spectra of THPP (5×10^{-6} mol L^{-1}) in the presence of HSA at pH 3.0. [HSA]: (1) 0, (2) 3.33×10^{-6}, (3) 6.67×10^{-6}, (4) 1.17×10^{-5}, (5) 2×10^{-5}, (6) 2.83×10^{-5}, (7) 3.67×10^{-5}, (8) 4.5×10^{-5}, (9) 6.17×10^{-5}, (10) 7×10^{-5} mol L^{-1}.

than the cationic, form of THPP with HSA through the van der Waals, hydrogen bonding, and hydrophobic interactions. Upon addition of HSA to the THPP solution, the neutral THPP is preferentially bound to HSA, which shifts the equilibrium to recover the concentration of neutral THPP, leading to the decrease of absorbance at 447 nm (the acidic form) and the increase at 425 nm (the neutral form).

Fluorescence titration was performed at a fixed THPP (5.0×10^{-6} mol L^{-1}) and varying HSA concentrations in a buffer solution at pH 3.0 with an excitation wavelength at 449 nm, and the results are shown in Fig. 3. In the absence of HSA, a fluorescence peak appeared at 712 nm, which is assignable to the acidic form of THPP. With increasing HSA concentration, the emission intensity of the acidic form gradually decreased and a new emission, assignable to the neutral THPP-bound to HSA, emerged at 660 nm with an apparent isoemissive point at 680 nm (Fig. 3a, right). The fluorescence excitation spectra (Fig. 3a, left) nicely coincided with the UV–vis spectra of THPP at all HSA concentrations, confirming that HSA and a neutral THPP form a complex. Selective excitation of the bound THPP at 423 nm gave a single fluorescence peak at 660 nm, intensity of which was remarkably enhanced by increasing the HSA concentration (Fig. 3b). The ultimate fluorescence intensity

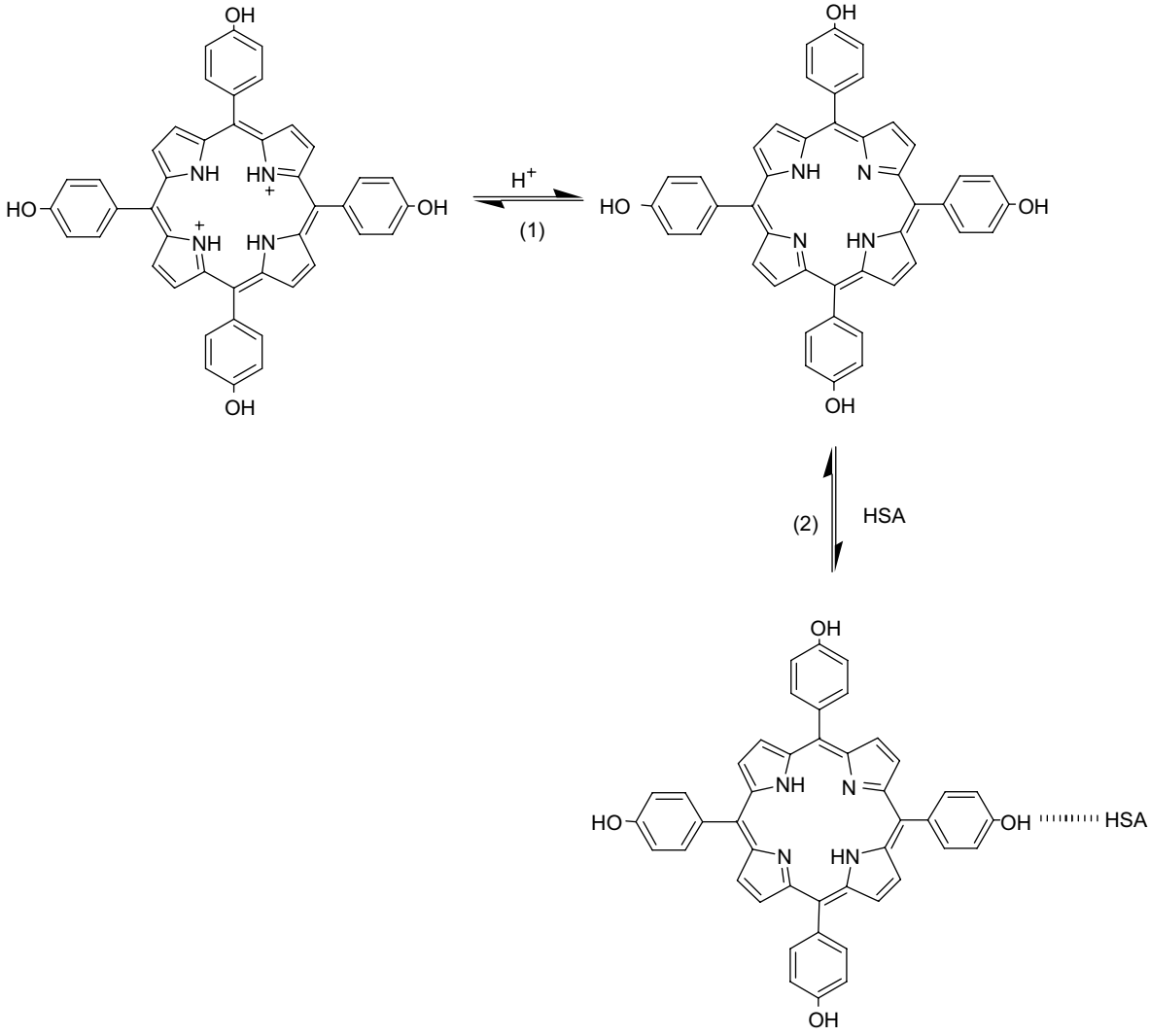

Scheme 1. The equilibria of (1) the acidic form and the neutral form of THPP, and (2) the neutral form of THPP and the THPP–HSA complex (the dashed line between THPP and HSA stands for the non-covalent interactions).

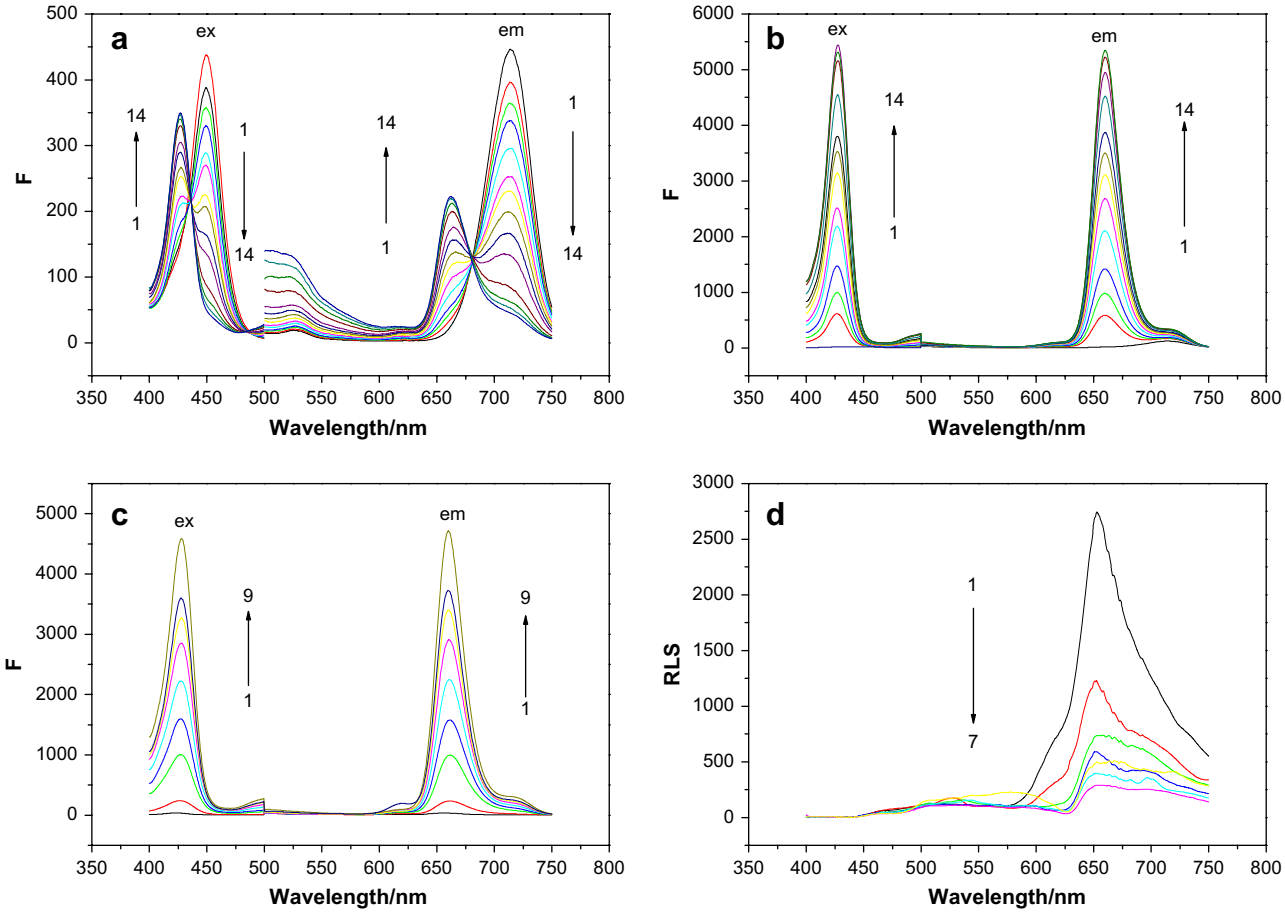

Fig. 3. Fluorescence spectra of THPP (5×10^{-6} mol L^{-1}) in the presence of HSA at pH 3.0: (a) $\lambda_{ex} = 449$ nm; (b) $\lambda_{ex} = 423$ nm; [HSA]: (1) 0, (2) 1.7×10^{-7}, (3) 3.4×10^{-7}, (4) 6.8×10^{-7}, (5) 1.2×10^{-6}, (6) 1.7×10^{-6}, (7) 2.6×10^{-6}, (8) 3.4×10^{-6}, (9) 5.1×10^{-6}, (10) 8.5×10^{-6}, (11) 1.7×10^{-5}, (12) 2.6×10^{-5}, (13) 3.4×10^{-5}, (14) 4.3×10^{-5} mol L^{-1}; (c) fluorescence spectra of THPP (5×10^{-6} mol L^{-1}) in the presence of HSA at pH 7.0: (1) 0, (2) 1.7×10^{-7}, (3) 6.7×10^{-7}, (4) 1.2×10^{-6}, (5) 1.7×10^{-6}, (6) 2.5×10^{-6}, (7) 3.3×10^{-6}, (8) 4.9×10^{-6}, (9) 8.3×10^{-6}, (10) 1.7×10^{-5}, (11) 2.5×10^{-5}, (12) 3.3×10^{-5} mol L^{-1}; (d) the resonance light scattering (RLS) spectra of THPP (5×10^{-6} mol L^{-1}) in the presence of HSA at pH 7.0: (1) 0, (2) 1.7×10^{-7}, (3) 6.7×10^{-7}, (4) 1.2×10^{-6}, (5) 3.3×10^{-6}, (6) 8.3×10^{-6}, (7) 3.3×10^{-5} mol L^{-1}.

observed for the HSA-bound neutral THPP was 300 times stronger than the original fluorescence of HSA-free cationic THPP. It should be emphasized that the fluorescence of HSA-bound neutral THPP develops at 660 nm almost from the zero level and can be detected in high sensitivity and accuracy, without any interference by the fluorescence of cationic THPP which appears only at longer wavelengths. Thus, THPP is a promising candidate of fluorescence sensor for HSA and other transport proteins.

At pH 7.0 (Fig. 3c), upon excitation of THPP at 423 nm, remarkable fluorescence enhancement at around 660 nm was induced by adding HSA, implying the formation of THPP–HSA complex. Obviously, the same fluorescence maxima of THPP at pH 3.0 and 7.0 indicate the complexation of neutral THPP to HSA. This is quite reasonable, as the neutral THPP is more hydrophobic than the charged acidic or basic form and is readily accommodated in the hydrophobic pocket of HSA. Furthermore, the resonance light scattering (RLS) [31] experiments (Fig. 3d) revealed the non-aggregating nature of both the free cationic THPP and HSA-bound neutral THPP, exhibiting no enhanced scattering peak at the major Soret band region.

3.2. Effect of pH on the binding of THPP to HSA

Fig. 4 represents the effect of pH from 2.0 to 11.0 on the fluorescence spectra of THPP in the absence and presence of HSA. In the absence of HSA (Fig. 4a), there are three forms of THPP: the acidic form (pH < 3.0, λ_{em} 715 nm), the neutral form (pH from 4.0 to 10.0, λ_{em} 660–663 nm) and the basic form (pH > 10.0, λ_{em} 638 nm). In the pH range of 2–10, the λ_{em} of THPP in the presence of HSA is almost identical at 660 nm, indicating that THPP is bound to HSA in its neutral form. At pH 11.0, the λ_{em} of THPP in the presence of HSA moved to 636 nm, suggesting that HSA binds the basic form of THPP. The fluorescence intensity of the THPP–HSA complex showed a dramatic dependence on solution pH (Fig. 4b). The pH dependence pattern of fluorescence intensity in the absence of HSA is similar to that observed for the fluorescence peak position. Thus, the fluorescence intensity is moderate at pH 2–3, but becomes extremely low at pH 4–10, and then revives to some extent at pH 11. In contrast, the fluorescence intensity is substantially enhanced in the presence of HSA, excepting that at pH 2, and varies dynamically depending on pH, most probably due to the absorbance change at the chosen excitation wavelength. Nevertheless, the intensity at pH 11 is more or less smaller than that at pH 3–10 as was the case with the fluorescence maximum, again excepting the value at pH 2, where only a small amount of neutral form is bound to THPP.

3.3. Binding constants of the THPP–HSA complex

In order to quantitatively examine the interaction of THPP with the protein, the binding constants were determined from the fluorescence intensity changes by using the following equation reported by Bhattacharya et al. [32].

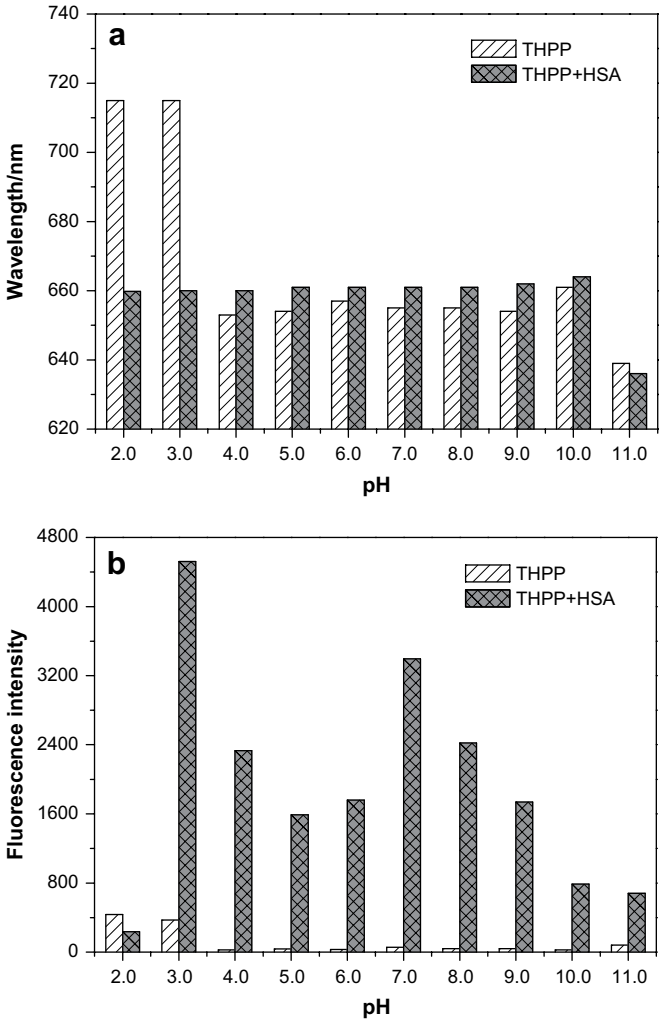

Fig. 4. Effect of pH on the interaction of THPP with HSA at pH 2.0–11.0. [THPP] = 5×10^{-6} mol L^{-1}, [HSA] = 5×10^{-6} mol L^{-1}. (a) Fluorescence peak, (b) fluorescence intensity.

$$\frac{1}{\Delta F} = \frac{1}{\Delta F_{max}} + \frac{1}{K[Q]}\left(\frac{1}{\Delta F_{max}}\right) \quad (1)$$

where $\Delta F = F_X - F_0$ and $\Delta F_{max} = F_\infty - F_0$, in which F_0, F_X and F_∞ are the fluorescence intensities of THPP in the absence of HSA, at an intermediate concentration of HSA, and at the saturation of interaction, respectively. Table 1 summarizes the binding constants (K_1) of THPP with HSA at pH 3.0 and 7.0 based on Eq. (1), respectively.

3.4. Quenching of the intrinsic fluorescence of HSA

The quenching of HSA fluorescence was performed at pH 3.0 in the presence of THPP at various concentrations, and the results are shown in Fig. 5. The fluorescence intensity of HSA gradually decreased with increasing THPP concentration. The excitation and emission maxima were observed at 281 and 349 nm, respectively.

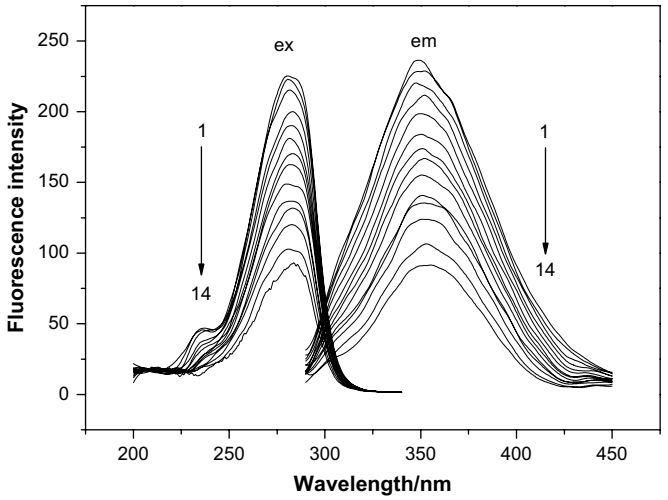

Fig. 5. The quenching of intrinsic HSA fluorescence by THPP. [THPP]: (1) 0, (2) 1.0×10^{-6}, (3) 2.0×10^{-6}, (4) 3.0×10^{-6}, (5) 5.0×10^{-6}, (6) 7.0×10^{-6}, (7) 9.0×10^{-6}, (8) 1.0×10^{-5}, (9) 1.2×10^{-5}, (10) 1.5×10^{-5}, (11) 1.7×10^{-5}, (12) 2.0×10^{-5}, (13) 2.5×10^{-5}, (14) 3.0×10^{-5} mol L^{-1}.

Addition of THPP caused a noticeable decrease in HSA fluorescence intensity. Meanwhile, the maximum emission wavelength showed a small bathochromic shift from 349 to 355 nm and the corresponding excitation wavelength slightly shifts from 281 to 285 nm.

It is well known that quenching occurs through the static or dynamic quenching process, both of which can result in a linear Stern–Volmer plot. To analyze the data from the quenching experiments, we used the Stern–Volmer equation:

$$\frac{F_0}{F} = 1 + K_{SV}[Q] = 1 + K_q\tau_0[Q] \quad (2)$$

where F and F_0 are the fluorescence intensities in the presence and absence of a quencher, respectively. K_{SV}, K_q, τ_0 and [Q] denote Stern–Volmer constant, quenching rate constant, the original lifetime of HSA and the concentration of quencher, respectively. According to Eq. (2), the Stern–Volmer constants (K_{SV}) were calculated from the slope of Fig. 6 and the results are listed in Table 1.

It is generally accepted that the maximum Stern–Volmer constant allowed for the dynamic quenching of biomolecules is 100 L mol^{-1}. Clearly, the Stern–Volmer constant obtained for THPP is two orders of magnitude greater than 100 L mol^{-1}. It is concluded therefore that the quenching is not a dynamic but static process occurring in the THPP–HSA complex. So the K_2 (binding constant) and n (binding site) can been calculated by the following equation.

$$\lg\frac{(F_0 - F)}{F} = \lg K + n \lg[Q] \quad (3)$$

where F_0 and F represent fluorescence intensities in the absence and presence of THPP, respectively, and [Q] the concentration of the quencher. The quenching processes at pH 3.0 and 7.0 seem similar. The Stern–Volmer plots, as well as the values of K_2 and n at pH 3.0 and 7.0 are shown in Fig. 6 and Table 1, respectively.

Table 1
Binding constants (K_1, K_2), number of binding sites (n), and distance (r) between THPP and Trp^{214} at pH 3.0 and pH 7.0

pH	$K_1/10^5$ M^{-1}	$K_{SV}/10^4$ M^{-1}	$K_2/10^5$ M^{-1}	n	$J/10^{14}$ cm^3 mol^{-1} L	R_0/nm	E	r/nm
3.0	7.50 ± 0.92	6.12 ± 0.22	1.40 ± 0.07	1.10	3.93	2.97	0.160	3.91
7.0	1.55 ± 0.41	7.38 ± 0.25	0.25 ± 0.06	0.93	5.09	3.31	0.196	4.18

K_1, K_{SV}, J, R_0, E and r values were obtained by using Eqs. (1), (2), (6), (5), (7) and (4), respectively; while K_2 and n by Eq. (3).

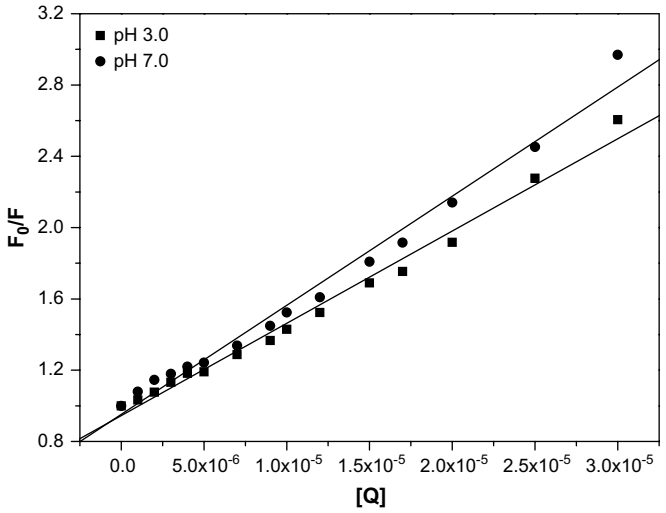

Fig. 6. The Stern–Volmer plots for the quenching of HSA by THPP at pH 3.0 and 7.0.

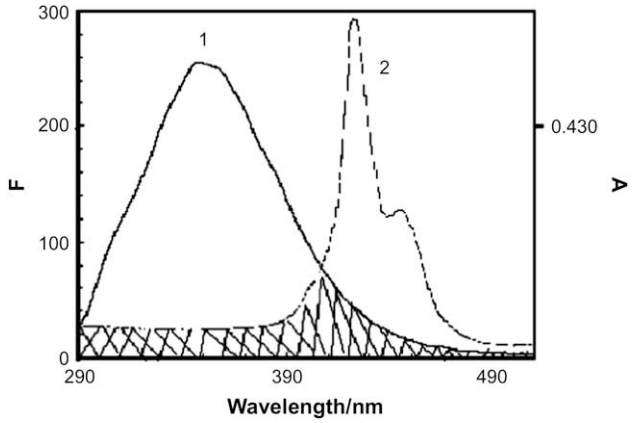

Fig. 7. Overlap of the fluorescence spectrum of HSA (1) with the absorption spectrum of THPP (2) at pH 3.0.

3.5. Energy transfer between THPP and HSA

Based on the Förster dipole–dipole non-radiative energy transfer theory [33,34], the energy transfer will occur under the following conditions: (1) the donor can emit fluorescence; (2) the emission spectrum of the donor and the UV–vis spectrum of the acceptor overlap to each other; and (3) the distance between the donor and the acceptor is shorter than 7 nm. The energy transfer efficiency (E) is related not only to the distance between the acceptor and donor (r), but also to the critical energy transfer distance (R_0), that is:

$$E = R_0^6/\left(R_0^6 + r^6\right) \tag{4}$$

where R_0 is the critical distance when the transfer efficiency is 50%.

$$R_0^6 = 8.8 \times 10^{-25} K^2 N^{-4} \Phi J \tag{5}$$

where K^2 is the spatial orientation factor of the dipole, N the refractive index of the medium, Φ the fluorescence quantum yield of the donor, J the overlap integral of the fluorescence emission spectrum of the donor and the absorption spectrum of the acceptor. Therefore,

$$J = \sum F(\lambda)\varepsilon(\lambda)\lambda^4 \, \mathrm{d}\lambda / \sum F(\lambda)\mathrm{d}(\lambda) \tag{6}$$

where $F(\lambda)$ is the fluorescence intensity of the fluorescent donor at wavelength λ and $\varepsilon(\lambda)$ the molar extinction coefficient of the acceptor at wavelength λ.

The energy transfer efficiency, E, is given by

$$E = 1 - F'/F \tag{7}$$

where F and F' represent the fluorescence intensities of the donor in the absence and presence of the acceptor, respectively.

The overlap of the absorption spectrum of THPP and the fluorescence spectrum of HSA at pH 3.0 is shown in Fig. 7. The parameter J was evaluated by integrating the spectra over $\lambda = 290$–500 nm. R_0 was obtained from Eq. (5) with $K^2 = 2/3$ and $N = 1.336$ [26]. The quantum yield $\Phi = 0.0955$ (pH 3.0) of the tryptophan in HSA is determined by comparison under the same excitation and instrumental parameters, using L-Trp as a standard substance ($\Phi_{\text{L-Trp}} = 0.14$ [35]) and measuring the fluorescence intensities ($F_{\text{L-Trp}}$ and F_{HSA}) and absorbance values ($A_{\text{L-Trp}}$ and A_{HSA}) of the most dilute solution ($A < 0.05$) of L-Trp and HSA, then Φ_{HSA} being calculated by the following equation [36]:

$$\Phi_{\text{HSA}} = \Phi_{\text{l-Trp}} \times \frac{F_{\text{HSA}}}{F_{\text{l-Trp}}} \times \frac{A_{\text{l-Trp}}}{A_{\text{HSA}}}.$$

The distances between THPP and the tryptophan residue [37] in HSA (r) were calculated by Eq. (4) based on the energy transfer efficiency E obtained from Eq. (7). Obviously, the r values (Table 1) are smaller than 7 nm upon complexation of THPP to HSA, which indicates that the quenching of HSA fluorescence by THPP is a static process obeying Förster's non-radiative energy transfer theory [33,34]. All related calculation results are summarized in Table 1.

3.6. Changes of the secondary structure of HSA induced by the binding of THPP

For better understanding the binding of THPP to HSA, the FT-IR spectroscopy was employed. The infrared spectra of proteins exhibit the amide bands, which represent the different vibrations of the peptide moiety. Of these amide bands, the amide I is most frequently used for characterizing the protein's secondary structure, due to its high sensitivity to the structural changes [21,38]. This band originates principally from the C=O stretching vibration of the amide group and appears in the region between 1600 and 1700 cm^{-1} [39].

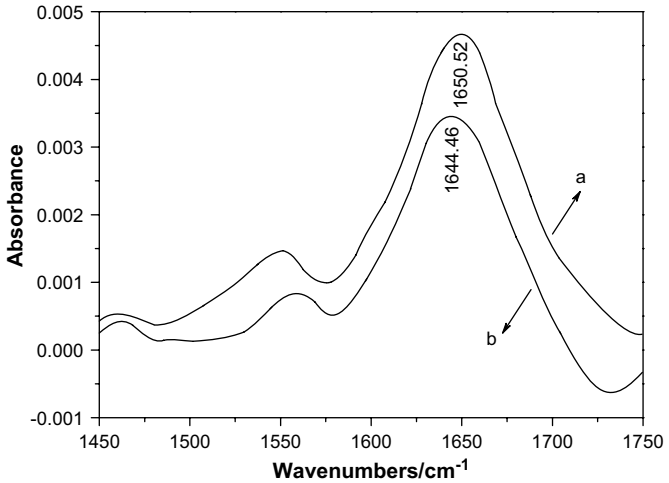

Fig. 8. FT-IR spectra and different spectra of HSA in aqueous solution: (a) FT-IR spectrum of HSA, (b) FT-IR difference spectrum of HSA obtained by subtracting the spectrum of the THPP solution from that of the THPP–HSA solution at 298 K, pH 7. 0; $[\text{HSA}] = 1.5 \times 10^{-6}$ mol L^{-1}, $[\text{THPP}] = 3.0 \times 10^{-6}$ mol L^{-1}.

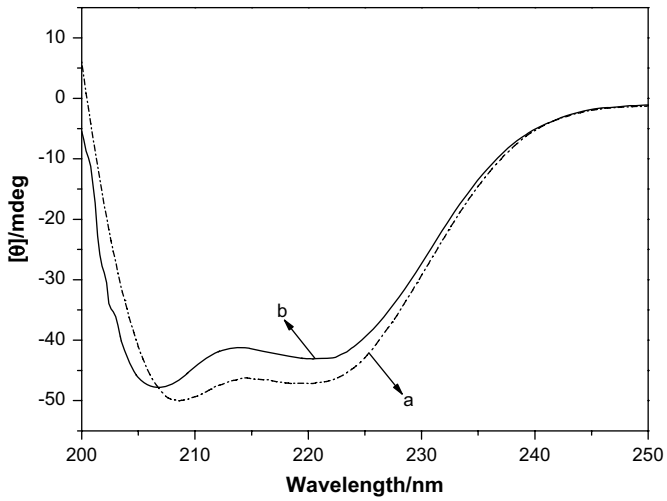

Fig. 9. CD spectra of the THPP–HSA system. (a) 1.5×10^{-6} mol L^{-1} HSA, (b) 1.5×10^{-6} mol L^{-1} HSA + 3.0×10^{-6} mol L^{-1} THPP. $T = 298$ K, pH 7.0.

The FT-IR difference spectra of the THPP-free and THPP-bound HSA in pH 7.0 (Fig. 8) showed an appreciable shift of the amide I band from 1650.5 to 1644.5 cm^{-1} and a decrease in intensity. The IR self-deconvolution with second-derivative resolution enhancement and curve-fitting procedure were used for a quantitative analysis of the secondary structure of HSA before and after the interaction with THPP. According to the well-established assignment criterion [40], the component bands at 1650–1660 cm^{-1} are assigned to α-helix. The results indicate that the α-helix content of HSA is reduced by ca. 9% upon complexation with THPP.

In addition, CD spectroscopy was applied to analyze the change of HSA's secondary structure in the absence and presence of THPP. The CD spectrum of free HSA in pH 7.0 solution (Fig. 9) exhibits the characteristic features of the α-helical structure of protein with negative bands in the UV region at 208 and 222 nm. The binding of THPP to HSA caused a decrease in negative ellipticity at all wavelengths and a slight shift of the peaks, indicating that THPP induces a slight decrease in the α-helix structure content of the protein. The calculating results exhibited a 7% reduction of α-helix structure, which coincides with the result from the IR study.

From the above results, it is apparent that the binding of THPP to HSA causes a conformational change of the protein, i.e., a reduction of α-helix structure. Similarly, Zhang et al. [21] reported that the binding of naringin to HSA leads to a reduction of the α-helix content in HSA, and the main interaction between them is hydrophobic force. On the contrary, it was reported that the binding of vitamin B_{12} to the surface of HSA induces an increase of α-helicity of the protein, which means that the interaction stabilized the structure of HSA in solution [41], and it was suggested that the main driving force is electrostatic in nature. In the present case, we observed a reduction of α-helicity of HSA upon complexation of THPP and therefore deduce that the binding of THPP to HSA makes the tertiary structure of HSA looser to some extent, which may be driven by the insertion of THPP to the hydrophobic cleft of HSA mainly through the hydrophobic interaction. This conclusion is consistent with that from the fluorescence and molecular modeling studies.

3.7. Molecular modeling

Molecular modeling method has been employed to promote the understanding of the interaction of drugs and HSA [21,22,42]. The 3D structure of crystalline albumin [43] has revealed that HSA comprises of three homologous domains that assemble to form a heart-shaped molecule. HSA is monomeric but contains the three structurally similar helical domains (I–III); each domain has two subdomains (A and B), which have six (A) and four (B) α-helices, respectively. The principal ligand-binding regions of HSA are located in the hydrophobic cavities of subdomains IIA and IIIA, called site I and site II, respectively, and one tryptophan residue (Trp^{214}) of HSA exists in subdomain IIA. Recent studies have shown that HSA is able to bind multiple ligands in several binding sites [44,45]. The crystal structure of the HSA complex of halothane, one of the most widely used general anesthetics, was taken from the Brookhaven Protein Data Bank (entry codes 1E78) [43]. The potential of the 3D structure of HSA was assigned according to the CFF91 force field. The initial structures of all the molecules were generated by molecular modeling platform Insight II 2000 (Accelrys). The geometries of these compounds were subsequently optimized using the CFF91 force field. Discover 3.0 program was applied to calculate the possible conformations of the ligands that bind to the protein. Based on this kind of approach a computational

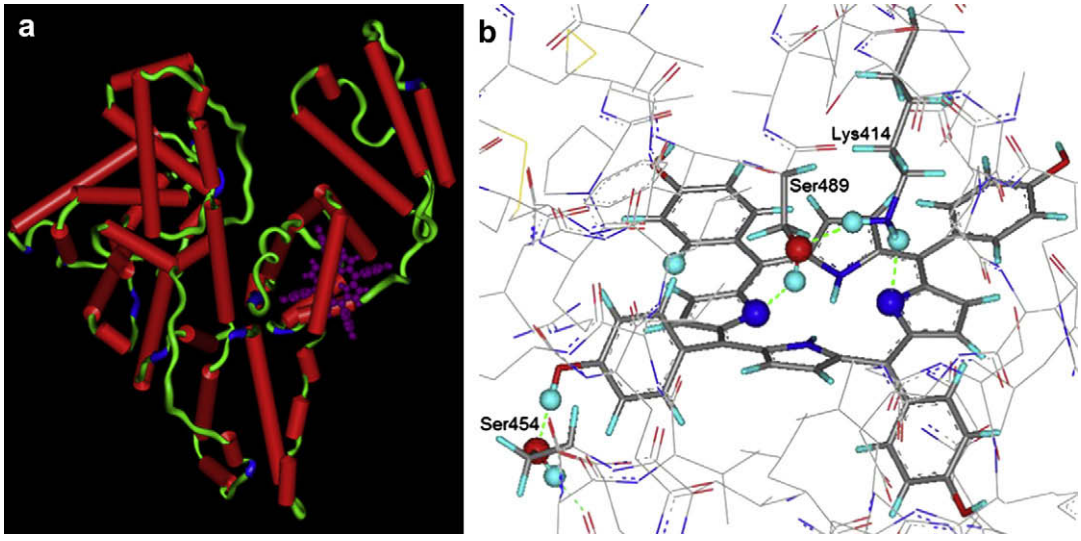

Fig. 10. (a) The binding mode of THPP with HSA. (b) Only those residues that are located around THPP are displayed. The amino acid residues forming hydrogen bonds are drawn by stick model, the other residues by wire model and THPP by stick model. Atoms directly forming hydrogen bonds are represented by ball model, and the hydrogen bonds are shown by dashed lines.

model of the target–receptor was built, all binding parameters of the THPP–HSA system were calculated on SGI workstations. The best energy ranked result of the binding mode of THPP with HSA is shown in Fig. 10.

As shown in Fig. 10a, THPP is partially accommodated in the subdomain IIIA of the protein. Two of the hydroxyphenyls are located within the binding pocket and the other two hydroxyphenyls stretch out of it. The porphyrin ring of THPP is kept coplanar. On the other hand, there are three hydrogen bonds formed between THPP and HSA (Fig. 10b). Thus, the non-protonated nitrogen atoms of neutral porphyrin are connected to the hydrogens of Ser^{489} and Lys^{414} of HSA, and one of the phenolic hydrogens of THPP to the oxygen atom of Ser^{454} of HSA. The formation of hydrogen bonds increases the stability of the THPP–HSA system. The results obtained from molecular modeling indicate that the binding of THPP with HSA is dominated by hydrophobic force, with the cooperation of hydrogen bonds between THPP and the polar amino acid residues. The root-mean-square (RMS) difference value of the conformations of free and THPP-bound HSA is 1.04, suggesting the slight change of the tertiary structure of HSA. The calculated distance between the center of THPP and Trp^{214} is about 3.6 nm, which is consistent with the spectroscopic results.

4. Conclusions

The present study revealed that (1) THPP is bound to HSA as a neutral species over a wide pH range of 2.0–10.0, indicating that the hydrophobic interaction is the major driving force for complexation, (2) subsequently, the binding constants of pH 3.0 and 7.0 differ by a factor of ~5, which suggests that the modulation of pH on the aggregate degree of THPP may be one of the important factors impacting the affinity of THPP to HSA, (3) the quenching of HSA fluorescence by THPP-bound near Trp^{214} is static in nature and occurs through the efficient Förster resonance energy transfer, (4) the FT-IR and CD spectral examinations revealed that the binding of THPP to HSA induces a conformational change of HSA, leading to a reduction of α-helical structures of the protein, and (5) the molecular modeling study showed that THPP binds partially to HSA at the subdomain IIIA by hydrophobic and hydrogen bonding interactions to Ser^{489}, Ser^{454} and Lys^{414} of HSA, which reinforces the conclusions derived from the experimental work and further provides the structural information about the binding mode of THPP with HSA.

Acknowledgements

This work was supported by the Natural Science Foundation of China (No. 20575038) and the Youth Foundation of Shanxi Province (No. 2006021009).

References

[1] Bonnett R, Martínez G. Photobleaching of sensitizers used in photodynamic therapy. Tetrahedron 2001;57:9513–47.
[2] Lang K, Mosinger J, Wagnerová DM. Photophysical properties of porphyrinoid sensitizers non-covalently bound to host molecules; models for photodynamic therapy. Coordination Chemistry Reviews 2004;248:321–50.
[3] Andrade SM, Costa SMB. Spectroscopic studies on the interaction of a water soluble porphyrin and two drug carrier proteins. Biophysical Journal 2002;82:1607–19.
[4] Berenbaum MC, Akande SL, Bonnett R, Kaur H, Ioannou S, White RD, et al. *meso*-Tetra(hydroxyphenyl) porphyrins, a new class of potent tumor photosensitizers with favourable selectivity. British Journal of Cancer 1986;54:717–25.
[5] Lambrechts SAG, Aalders MCG, Verbraak FD, Lagerberg JWM, Dankert JB, Schuitmaker J. Effect of albumin on the photodynamic inactivation of microorganisms by a cationic porphyrin. Journal of Photochemistry and Photobiology B: Biology 2005;79:51–7.
[6] Gantchev TG, Ouellet R, Liter JEV. Binding interactions and conformational changes induced by sulfonated aluminum phthalocyanines in human serum albumin. Archives of Biochemistry and Biophysics 1999;366(1):21–30.
[7] Biesaga M, Pyrzynska K, Trojanowicz M. Porphyrins in analytical chemistry. A review. Talanta 2000;51:209–24.
[8] Liu J, Huang JW, Shen H, Wang H, Yu HC, Ji LN. The synthesis of two novel hybrids containing a zinc(II) porphyrin unit and a polypyridyl ruthenium(II) complex unit and their photoinduced intramolecular electron and energy transfer. Dyes and Pigments 2008;77(2):374–9.
[9] Dehghani H, Fathi F. Molecular complexation of *meso*-tetraphenyl porphyrins with SO_2. Dyes and Pigments 2008;77(2):323–6.
[10] Han FX, Wheelhouse RT, Hurley LH. Interactions of TMPyP4 and TMPyP2 with Quadruplex DNA. Structural basis for the differential effects on telomerase inhibition. Journal of the American Chemical Society 1999;121:3561–70.
[11] Wang XP, Pan JH, Yang XD, Niu CD, Zhang Y, Shuang SM. Porphyrin binding to DNA investigated by cyclodextrin supramolecular system. Analytical and Bioanalytical Chemistry 2002;374:445–50.
[12] Rovers JP, Saarnak AE, Molina A, Schuitmaker JJ, Sterenborg HJCM, Terpstra OT. Effective treatment of liver metastases with photodynamic therapy, using the second-generation photosensitizer *meta*-tetra(hydroxyphenyl)chlorin (mTHPC), in a rat model. British Journal of Cancer 1999;81:600–8.
[13] Petitpas I, Bhattacharya AA, Twine S, East M, Curry S. Crystal structure analysis of warfarin binding to human serum albumin – anatomy of drug site I. Journal of Biological Chemistry 2001;276(25):22804–9.
[14] Galántai R, Nagy IB, Módos K, Kardos J, Závodszky P, Fidy J. Serum albumin–lipid membrane interaction influencing the uptake of porphyrins. Archives of Biochemistry and Biophysics 2000;373(1):261–70.
[15] Il'ichev YV, Perry JL, Simon JD. Interaction of ochratoxin A with human serum albumin. Preferential binding of the dianion and pH effects. Journal of Physical Chemistry B 2002;106:452–9.
[16] Kubat P, Lang K, Anzenbacher P. Modulation of porphyrin binding to serum albumin by pH. Biochimica et Biophysica Acta 2004;1670:40–8.
[17] Cohen S, Margalit R. Binding of porphyrin to human serum albumin. Structure–activity relationships. Biochemical Journal 1990;270:325–30.
[18] Chatterjee S, Srivastava TS. Spectral investigations of the interaction of some porphyrins with bovine serum albumin. Journal of Porphyrins and Phthalocyanines 2000;4:147–57.
[19] Rotenberg M, Margalit R. Deuteroporphyrin–albumin binding equilibrium – the effects of porphyrin self-aggregation studies for the human and the bovine proteins. Biochemical Journal 1985;229:197–203.
[20] Borissevitch IE, Tominaga TT, Imasato H, Tabak M. Resonance light scattering study of aggregation of two water soluble porphyrins due to their interaction with bovine serum albumin. Analytica Chimica Acta 1997;343:281–6.
[21] Zhang YH, Li Y, Dong LJ, Li JZ, He WY, Chen XG, et al. Investigation of the interaction between naringin and human serum albumin. Journal of Molecular Structure 2008;875(1–3):1–8.
[22] He WY, Li Y, Si HZ, Dong YM, Sheng FL, Yao XJ, et al. Molecular modeling and spectroscopic studies on the binding of guaiacol to human serum albumin. Journal of Photochemistry and Photobiology A: Chemistry 2006;182:158–67.
[23] Zhang WB, Zhang LH, Ping GC, Zhang YK, Kettrup A. Study on the multiple sites binding of human serum albumin and porphyrin by affinity capillary electrophoresis. Journal of Chromatography B 2002;768(1):211–4.
[24] Yushmanov VE, Tominaga TT, Borissevitch IE, Imasato H, Tabak M. Binding of manganese and iron tetraphenylporphine sulfonates to albumin is relevant to their contrast properties. Magnetic Resonance Imaging 1996;14(3):255–61.
[25] Wang YP, Wei YL, Dong C. Study on the interaction of 3,3-bis (4-hydroxy-1-naphthyl)-phthalide with bovine serum albumin by fluorescence spectroscopy. Journal of Photochemistry and Photobiology A: Chemistry 2006;177:6–11.
[26] Pang YH, Yang LL, Shuang SM, Dong C, Thompson M. Interaction of human serum albumin with bendroflumethiazide studied by fluorescence spectroscopy. Journal of Photochemistry and Photobiology B: Biology 2005;80:139–44.
[27] Guo XL, An WT, Shuang SM, Cheng FQ, Dong C. Study on the spectroscopic characterization of *meso*-tetrakis (4-hydroxyphenyl) porphyrin (THPP) in β-cyclodextrin and its derivatives. Journal of Photochemistry and Photobiology A: Chemistry 2005;173:258–63.
[28] Dong AC, Huang P, Caughey WS. Protein secondary structure in water from second-derivative amide I infrared spectra. Biochemistry 1990;29(13):3303–8.
[29] Wei YJ, Li KA, Tong SY. Spectral study of interaction of thymol blue with protein in acidic solution. Analytica Chimica Acta 1997;341:97–104.
[30] Horton HR, Moran LA, Ochs RS, Rawn JD, Scrimgeour KG. Principle of biochemistry. 3rd ed., photocopy edition. Beijing, China: Science Press; 2003. p. 31–3.
[31] Pasternack RF, Collings PJ. Resonance light scattering: a new technique for studying chromophore aggregation. Science 1995;269:935–9.
[32] Bhattacharya J, Bhattacharya M, Chakraborty A, Chowdhury U, Podder RK. Interaction of chlorpromazine with myoglobin and hemoglobin. A comparative study. Biochemical Pharmacology 1994;47:2049–52.
[33] Lakowicz JR. Principle of fluorescence spectroscopy. New York, USA: Plenum Press; 1983. p. 367–94.
[34] Leibowitz M. Remarks on Förster's theory of transfer of excitation energy. Journal of Physical Chemistry 1965;69(3):1061–2.
[35] Yang MM, Yang P, Zhang LW. Study on interaction of caffeic acid series medicine and albumin by fluorescence method. Chinese Science Bulletin 1994;39(9):734–9.
[36] Wu PG, Brand L. Resonance energy transfer: methods and applications. Analytical Biochemistry 1994;218(1):1–13.
[37] Stryer L. Fluorescence energy transfer as a spectroscopic ruler. Annual Review of Biochemistry 1978;47:819–46.
[38] Rahmelow K, Hubner W. Secondary structure determination of proteins in aqueous solution by infrared spectroscopy: a comparison of multivariate data analysis methods. Analytical Biochemistry 1996;241(1):5–13.

[39] Witold KS, Henry HM, Dennis C. Determination of protein secondary structure by Fourier transform infrared spectroscopy: a critical assessment. Biochemistry 1993;32(2):389–94.
[40] Surewicz KW, Mantsch HH. New insight into protein secondary structure from resolution-enhanced infrared spectra. Biochimica et Biophysica Acta 1988;952:115–30.
[41] Hou HN, Qi ZD, OuYang YW, Liao FL, Zhang Y, Liu Y. Studies on interaction between vitamin B12 and human serum albumin. Journal of Pharmaceutical and Biomedical Analysis 2008;47:134–9.
[42] Miskovsky P, Hritz J, Cortes SS, Fabriciova G, Ulicny J, Chinsky L. Interaction of hypericin with serum albumins: surface-enhanced Raman spectroscopy, resonance Raman spectroscopy and molecular modeling study. Photochemistry and Photobiology 2001;74(2):172–83.
[43] Bhattacharya AA, Curry S, Franks NP. Binding of the general anesthetics propofol and halothane to human serum albumin. Journal of Biological Chemistry 2000;275(49):38731–8.
[44] Lemiesz LT, Luczkowski M. Human serum albumin: spectroscopic studies of the paclitaxel binding and proximity relationships with cisplatin and adriamycin. Journal of Inorganic Biochemistry 2004;98:1851–6.
[45] Bocedi A, Notari S, Menegatti E, Fanali G, Fasano M, Ascenzi P. Allosteric modulation of anti-HIV drug and ferric heme binding to human serum albumin. FEBS Journal 2005;272:6287–96.